JSST
Journal of Space Science & Technology

Vol. 7/ No. 1/ 2014
pp. 13-24

Effects of Some Parameters on Thermal Control of a LEO Satellite

F. Farhani[1*] and A. Anvari[2]

1and 2. Department of Mechanical Engineering, Iranian Research Organization for Science and Technology (IROST)

[*]Postal Code: 158153538, Tehran, IRAN

f.farhani@irost.ir

Satellite thermal control ensures safe operating temperature ranges for satellite components throughout the mission life. Effects of altitude, spin, and position of satellite radiator(s) on the thermal control of a small Low Earth Orbit (LEO) satellite have been studied. Results show that change in satellite altitude, in the range considered here, does not produce critical thermal conditions. However, satellite spin rate has a marked influence on the satellite temperatures. Also, comparison of results for the satellite configurations considered in this study suggests that a radiator at top provides better thermal design conditions. Results also indicate the adequacy of the discussed considerations for use in the design of satellites of similar configurations, missions and orbital parameters.

Keywords: Altitude, beta angle, low earth orbit (LEO), satellite radiator, spin rate, thermal control

Nomenclature

A	area
C_i	heat capacity of node i
F_{i-j}	view factor from node i to node j
G	radiation conductor (defined in the text)
K	material conductivity
Q_i	heat dissipation of node i
ΣQ_{int}	total heat dissipated by the electronic components (internal heat dissipation)
T	temperature
α	absorptance
β	beta angle (defined as the angle between the orbit plane and the sun vector)
ε	emittance
σ	Stefan-Boltzmann constant
a	albedo
hot	hot
i, j	node indicators
int	internal
ir	infra red
max	maximum
s-s	satellite to space
DoD	Depth of Discharge
GMM	Geometrical Mathematical Model
LEO	Low Earth Orbit
RPO	Revolution Per Orbit
SIN	Systems Improved Numerical Differencing
TD	Thermal Desktop
TMM	Thermal Mathematical Model

Introduction

The duty of satellite thermal control system is to maintain the temperatures of satellite components and surfaces within allowable limits throughout the satellite mission. Active and passive thermal control methods are used for this purpose, which differ in some of the thermal hardware and control strategies they use to achieve the required thermal control action. However, the passive method is preferable, when simplicity, cost and reliability are the key design considerations [1, 2]. The passive thermal control is affected by parameters such as beta angle (the smaller angle between the sun vector and the plane of the satellite orbit), satellite altitude, satellite spin rate, and the position of the satellite radiator(s) [3]. These parameters must be considered in the thermal design process. However, there is little information in the

1. Assistant Professor (Corresponding Author)
2. M.Sc.

open literature on the effects of the above parameters on the thermal control of satellites. In the following sections, the importance of the above parameters are discussed in brief, following which, their effects on the thermal control of a Low Earth Orbit (LEO) satellite are presented in detail. The results, discussions and conclusions presented in this paper can be of help to thermal designers working on satellites of similar configurations, missions and orbital parameters.

Beta Angle

The beta angle determines the percentage of time an object such as a satellite in low Earth orbit (LEO) spends in direct sunlight, absorbing solar energy, and is defined as the angle between the orbit plane and the sun vector [4]. Figure 1 shows a pictorial presentation of the definition of the beta angle. It is the smaller angle between the sun vector and the plane of the satellite orbit. It should be noted that the beta angle does not define a unique orbit plane; all satellites in orbit with a given beta angle at a given altitude have the same exposure to the sun, even though they may be orbiting in completely different planes around the Earth [5]. The beta angle varies between +90° and −90°, and the direction the satellite revolves around the Earth determines whether the beta angle sign is positive or negative. Hence, viewing from the sun, a beta angle is positive if the satellite orbits in a counter clockwise direction and negative if it revolves clockwise [5]. The degree of orbital shadowing, which a satellite in LEO experiences, is determined by the satellite beta angle. A satellite launched into an initial orbit with an inclination equivalent to the complement to the Earth inclination with the ecliptic, results in an initial beta angle of 0 degrees (β = 0°) for the orbiting satellite. This allows the satellite to spend the maximum possible amount of its orbital period in the Earth's shadow, which results in an extremely reduced absorption of solar energy. At a LEO of 280 kilometers, the satellite in orbit is in sunlight through 59% of its orbit (approximately 53 minutes in sunlight, and 37 minutes in shadow [4]).

On the other extreme, a satellite launched into an orbit that follows the terminator, results in a beta angle of 90 degrees (β = 90°), and the satellite is in sunlight 100% of the time: an example would be a polar orbit initiated at local dawn or dusk on an equinox [6]. These orbits can be taken advantage of to keep a satellite as cool as possible for instruments that require low temperatures, such as infrared cameras, by keeping the beta angle as close to zero as possible, or conversely, to keep a satellite in sunlight as much as possible for conversion of sunlight by its solar panels, for solar stability of sensors, or to study the sun by maintaining a beta angle as close to +90 or -90º as possible [5].

In this paper, the satellite under study has been analyzed in various beta angles, ranging from 0 to 90º, and the satellite temperatures under these conditions have been obtained.

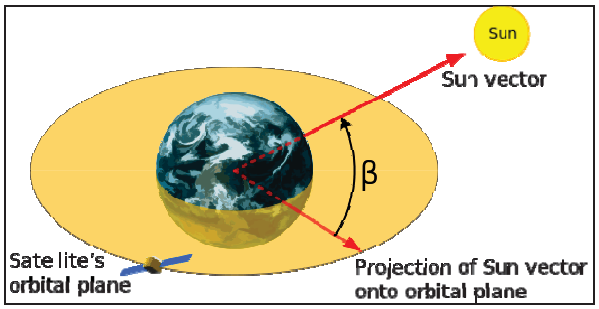

Fig. 1 Definition of Beta angle [3]

Satellite Altitude

For different orbital inclinations of a LEO satellite, altitude plays a major role in the determination of the β angle, which fixes the satellite position with respect to the sun and determines the orbit type (sun synchronous or asynchronous orbit). In addition, at a specific β angle, the satellite eclipse fraction depends on the satellite altitude [7]. Altitude also plays an important role in the determination of orbital period [8]. The eclipse fraction and orbital period, in turn, affect the satellite extreme temperatures and eclipse duration (battery discharge time), the sunlight duration (solar panel operation plus recharge time), and battery cycling (battery discharge time, solar panel operation plus recharge time). Eclipse fraction affects the battery temperature and *Depth of Discharge* (DoD). On the other hand, battery temperature determines battery isothermality, an important requirement of satellite batteries, which ensures that all cells charge and discharge at the same rate [1].

Altitude, as a pertinent orbital factor, also affects the amount and intensity of environmental factors such as solar intensity, particulate radiation, micrometeoroids and debris, and atomic oxygen [9, 10]. For example, the Earth environment, such as the amount of atomic oxygen that exists, varies with altitude changes.

Therefore, a clear understanding of the effects of variations in the altitude of a satellite can be very important to the designers of thermal control and electric power subsystems.

In this paper, the satellite under consideration has been analyzed in three different altitudes: 700, 893 and 1000 km, and in each case, temperatures for representing satellite surfaces have been obtained.

Satellite Spin

In the passive thermal control method, spinning of the satellite at an appropriate rate (*Revolution Per Orbit* (RPO)), about one of the satellite axis, can be used as a part of the overall thermal control strategy to ensure uniform temperatures on the external surfaces. Studies on rotating cylindrical space vehicles with body

mounted solar arrays [11-15] have shown the effect of spin rate on temperature distributions. Petrof [11] studied the effect of spin in minimizing the temperature peaks in a rotating vehicle. He concluded that, with increase in the rate of satellite spin, the extreme points of the surface temperature shift in the direction of the rotation, besides diminishing both maximum and minimum temperature values. In the limit, when the spin approaches infinity, the temperatures everywhere approach the average temperature of the vehicle as required by thermodynamic equilibrium. For example, for a cylindrical satellite spinning with the sun normal to the spin axis and having body mounted solar panels with solar absorption to infrared emittance ratio (α/ε) of nearly 1.0, the satellite will run around the room temperature [1]. Therefore, as reported by Gadalla [15], spinning of the satellite as it orbits the earth results in reduction in the overall temperature on the external surfaces of the satellite. This is especially important in the case of body mounted solar panels, because the rate of power production by the solar cells, as shown in Figure 2, is affected by their working temperatures [9-17].

In this paper, the satellite has been analyzed at several spin rates: RPO=1, 3, 5, and 10. The *No Spin* condition (RPO=0) and *Quick Spin* condition (RPO=∞) also have been analyzed as the limiting cases. For all the spins, temperatures of the satellite solar panels, considered as representative surfaces, have been obtained to show the effect of spin rate on the satellite temperatures.

Satellite Radiator(s) Position(s)

The external surfaces of a satellite radiatively couple the satellite to the deep space. These surfaces, known as radiators, are also exposed to external sources of energy such as direct solar, albedo (reflected solar flux) and Earth-emitted IR. Therefore, their radiative properties must be selected so that an energy balance at the desired temperature, between the satellite internal heat dissipation, external sources of heat, and re-radiation to space, is achieved. Radiators are given surface finishes, such as white paints with high infrared emittance ($\varepsilon > 0.8$) and low solar absorptance ($\alpha<0.2$), to maximize heat rejection from the radiators, while limiting the absorbed heat loads from the surroundings [10].

The heat removal can be arranged through one centralized radiator (all dissipated heat going to one centralized radiator) or several individual radiators, distributed in the satellite. For satellites with 3-axes stabilization, the choice of zone(s) for radiator(s) location(s) depends on the satellite orientation along its orbital movement. Hence, important issues that the satellite thermal designer must address pertain to determining the optimum position(s) of the radiator(s) on the satellite and estimating their size [3].

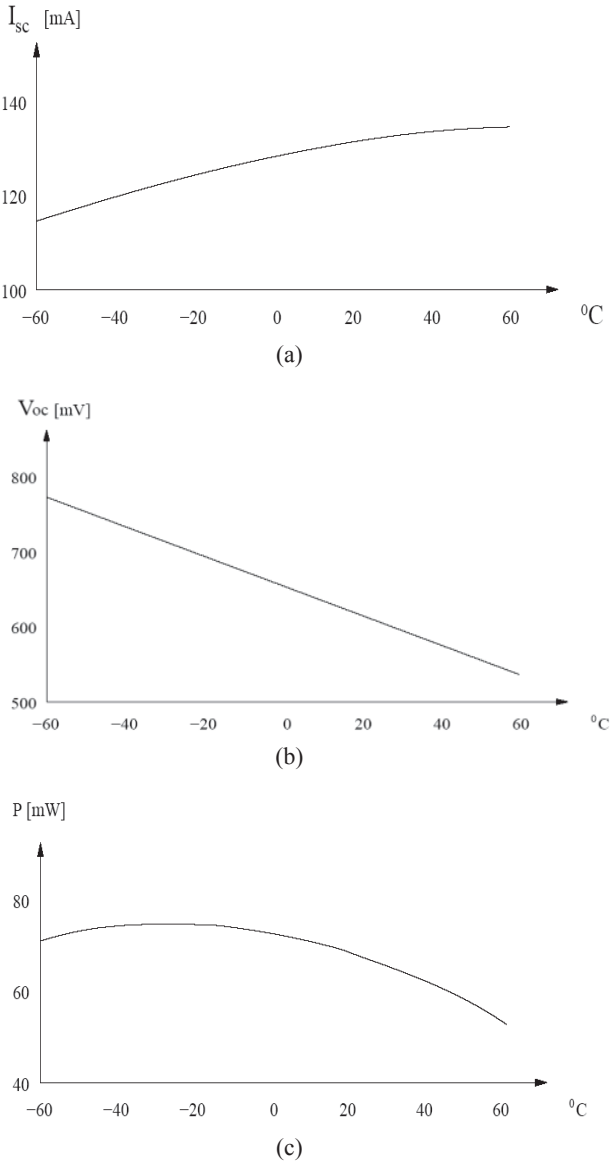

Fig. 2 Temperature effects on (a) short circuit current (b) open circuit voltage (c) maximum power of solar cells [9]

In order to size the radiator(s), the information on the satellite orbital positions, in relation to sun, is of great importance. The thermal designer must determine the paths, followed by the satellite during the course of the satellite mission, along which the impinging fluxes are the lowest and do not vary significantly. Regions that are mostly perpendicular to or shaded from the solar vector are candidate locations for placing the radiator(s). Other surfaces may have to be insulated to reduce the effects of exposure to space. These locations are also preferred from the viewpoint of improved predictability.

For an isothermal space facing radiator, with dissipating components mounted on its back (see Figure 3), the area A (one side) that will keep the temperature $T_{hot} \leq T_{max}$, where T_{hot} is the hot case temperature and

T_{max} is the maximum temperature considered acceptable for the radiator in orbit, is given by [18]:

$$A = \frac{\Sigma Q_{\text{int}}}{\varepsilon \sigma T^4 - \alpha\,(solar + albedo) + \varepsilon\,(IR)} \qquad (1)$$

where ΣQ_{int} is the total heat dissipated by the electronic components, and solar, albedo and (IR) are heat loads due to sun, albedo and Earth IR fluxes, respectively. Radiator temperature is sensitive to steadiness of the rejected power, and approximately 1 watt of energy produces about 1 K temperature change [19, 20].

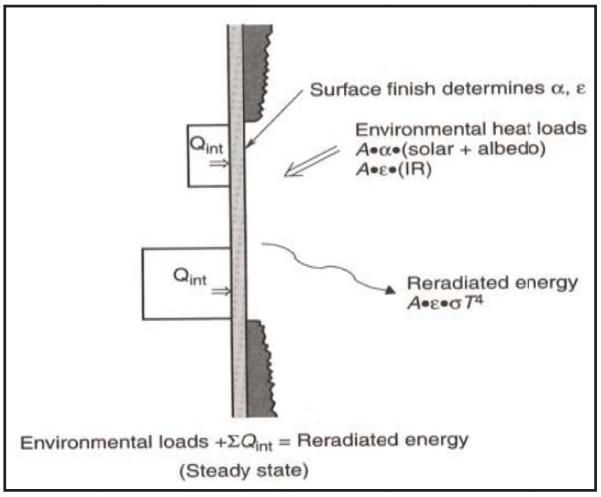

Fig. 3 Energy balance for the satellite radiator [1]

Considering the design heat loads, the radiator area calculated using Eq. (1) will give the thermal designer a rough idea about the optimum position(s) of satellite radiator(s). If a radiator is to be positioned on the top of the satellite (zenith oriented), the IR and albedo flux values will be zero, and radiator sized on the basis of Eq. (1) will run cold. On the other hand, for a radiator positioned at the bottom of the satellite (nadir oriented), the IR and albedo fluxes will be non-zero, assuming various values depending on the position of the satellite in the orbit. Whatever the case, a satellite radiator should have sufficient radiating area to fulfill its thermal duty. Therefore, it is important to estimate the required size and optimum position of satellite radiator(s) for any thermal control design.

In this paper, two configurations, namely top radiator configuration and bottom radiator configuration, have been analyzed to obtain the temperatures of the top and bottom surfaces of the satellite.

Thermal Modeling and Analysis

In this study, two specialized software, namely the *Systems Improved Numerical Differencing Analyzer* (SINDA), and the *Thermal Desktop software*, have been used for the satellite thermal modeling and analysis. SINDA, a network-style (resistor-capacitor circuit analogy) thermal simulator and heat transfer analysis software, uses lumped parameter modeling with FD method for heat transfer design. In general, a user poses a heat transfer problem by creating an arbitrary network of temperature points (*nodes*) connected by heat flow paths (*conductors)*. Thermal Desktop is a PC CAD-based thermal model builder.

As required by the thermal modeling process, more than 1000 lines of programming are also written for the construction and execution of the *Thermal Mathematical Model (TMM)*. Also, the detailed *Geometrical Mathematical Model (GMM)* of the satellite is constructed using the *Mechanical Desktop Environment*. It should be noted that these two models complement each other and both are necessary for the thermal modeling and analysis of a satellite.

The satellite components are modeled using the *Lumped Parameter Method*, where networks of temperature points (*thermal nodes*) connected by heat flow paths (*conductors)* are used to present each component in the nodal network. The component mass, optical and thermo-physical properties such as heat capacities are assumed to be concentrated in the center of the corresponding thermal nodes. In the present study, 500 thermal nodes are used for modeling various satellite components. The number of nodes, necessary to represent each component, is decided by the respective component criticality, i.e., its degree of importance to the satellite mission, and also the component sensitivity to orbital temperature variations.

The satellite thermal modeling and analysis process followed in this study consists of the following steps:

1. Constructing a *Geometrical Mathematical Model (GMM)* using *Thermal Desktop (TD) software*. This model (see Figure 5a, b) is used for the estimation of *view factors* and the absorbed *heat fluxes*, namely solar (Q_{sun}), albedo (Q_a) and Earth IR (Q_{ir}), which constitute the environmental thermal loads on the satellite.
2. Constructing a *Thermal Mathematical Model (TMM)*, consisting of linear and radiation conductors (see Figure 6a, b, c, d):
   a. The linear conductors, representing solid conduction, transport heat in direct proportion to the difference in nodal temperatures: $Q_{1\text{-}2} = G\,(T_1 - T_2)$, where $Q_{1\text{-}2}$ is the heat flowing from node 1 to node 2 through a conductor of value $G\ (= kA/\Delta x)$, T_1 is the current temperature of node 1, T_2 is the current temperature of node 2, K is the material conductivity, A is the internodal cross-sectional area and Δx is the distance from node to node center.

b. Radiation conductors transport heat according to the difference in the fourth power of absolute temperature: $Q_{1\text{-}2} = G\,(T_1^4 - T_2^4)$, with $G = \sigma\varepsilon_1 F_{1\text{-}2} A_1$, where σ is the Stefan-Boltzmann constant, ε_1 is the emissivity of node 1, A_1 is the area of node 1, and $F_{1\text{-}2}$ is the view factor from node 1 to node 2.

3. Creating the SINDA input file by writing the thermal network codes using a FORTRAN like language.
4. Arrangement of the *GMM* outputs, namely *view factors* and the *environmental heat fluxes*, which will be used in the *TMM*, in two files: (i) the first file containing data on the radiation conductors for radiation heat exchange among the internal surfaces and radiation between the external satellite surfaces and the deep space environment, and (ii) a second file containing the satellite environmental thermal loads.
5. Solving the resultant thermal network using SINDA, to obtain the satellite temperatures.

Figure 4 shows a schematic of a simple satellite model in its Earth orbit. The heat loads on the satellite are also shown. If there is a balance between the energies entering and leaving the satellite, the satellite will be at an equilibrium temperature, which can be determined by Eq. (2). This energy balance is defined by the energy emitted from the satellite to the deep space as infrared radiation ($Q_{s\text{-}s}$) on one hand, and the energy absorbed by the external satellite surfaces (Q_{sun}, Q_{ir}, Q_a) and the heat dissipation by the internal satellite components (Q_i), on the other. Therefore:

$$Q_{sun} + Q_{ir} + Q_a + Q_i = Q_{s-s} \tag{2}$$

It should be noted that all the terms in Eq. (2) may not be present simultaneously. For example, during an eclipse; Eq. (2) will be simplified by the elimination of the Q_{sun} and Q_a terms. Another important observation about Eq. (2) is that this equation only yields the temperature of the external surfaces of the satellite, and it does not provide any information about the satellite individual components or the local cold or hot spots. Therefore, in order to carry out a more detailed thermal analysis, it will be necessary to use a finer thermal network and a more accurate meshing scheme. In the view of the nonlinear nature of the resultant heat transfer partial differential equations, specialized software for thermal modeling and analysis are used in this study.

The SINDA code provides four methods, classified as *Steady State* and *Transient Methods*, for solving the equation network. The *Steady State* Methods are used for time independent cases, or as initial conditions for transient analyses. Transient subroutines are used to solve governing equations with respect to time.

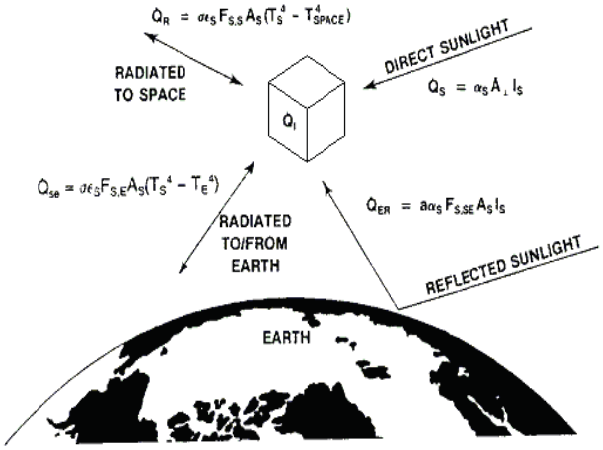

Fig. 4 Energy balance for a LEO satellite [2]

In the *Lumped Parameter Method*, the thermal network of the whole satellite is solved in such a way that at every time interval, the equation of conservation of energy is satisfied at each node in the network. The equation system, with the number of equations equal to the number of nodes in the network, has been analyzed numerically as an unsteady system, using a second order implicit numerical algorithm. The following equation, for the conservation of energy at thermal node *i*, holds:

$$C_i \frac{dT_i}{dt} = Q_i + \sum_{j=1}^{N} \{G_{ji}(T_j - T_i) + \hat{G}_{ji}(T_j^4 - T_i^4)\} \tag{3}$$

$$G_{ji} = \begin{cases} \dfrac{kA_{ij}}{l_{ij}} \\ K_{c,ij} A_{c,ij} \end{cases} \tag{4}$$

The radiation conductors are given as following:

$$\hat{G}_{ji} = \sigma\varepsilon_j F_{j-i} A_j \tag{5}$$

The small satellite considered in this analysis is cubical in shape: the bottom side faces the Nadir (towards the Earth), the top side faces the Zenith, and the four lateral sides are covered with solar panels. Figure 5a, b shows the satellite GMM models.

A passive thermal control system is designed in which paints, multilayer insulation (MLI), and passive structural radiators are incorporated. The radiators are painted white (emittance, ε>0.8, absorptance, α<0.2). Solar cells, placed on top of aluminum walls, are fixed on all lateral sides of the satellite.

Each thermal analysis set is performed by constructing two mathematical models: a geometrical mathematical model (GMM) (see Figure 5), consisting of sub-models such as electronic box, telemetry units, batteries, and the satellite structure, and a thermal mathematical model (TMM) (see Figure 6), consisting

of radiative and conductive thermal conductors. Output from a particular GMM, namely environmental heat fluxes consisting of solar, albedo and Earth IR, and radiative view factors, are used in the corresponding TMM to obtain the satellite temperatures.

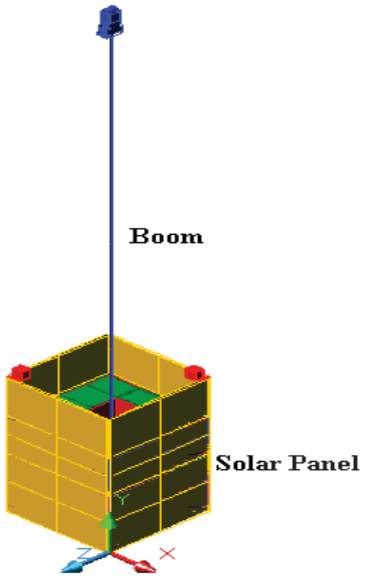

(a)

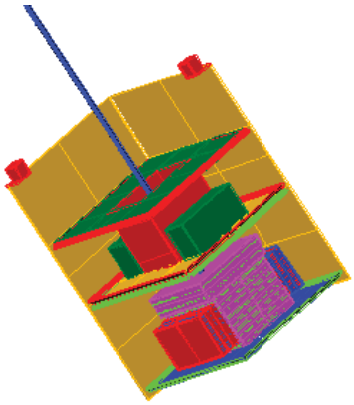

(b)

Fig. 5 GMM: (a) solar panels, (b) internal components

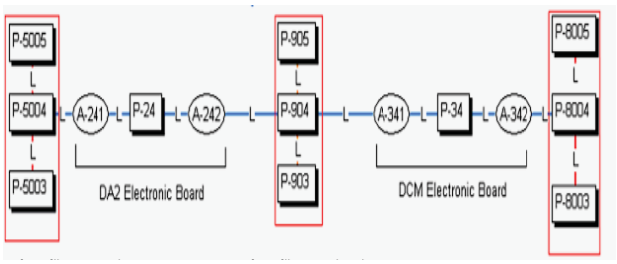

(a)

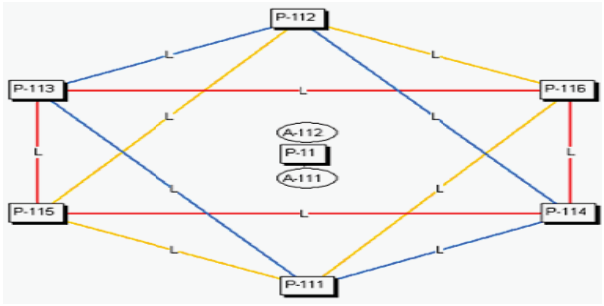

(b)

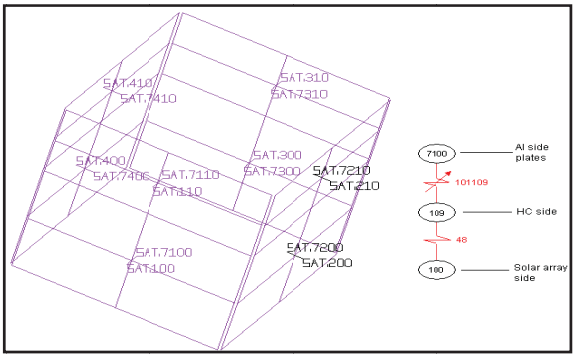

(c)

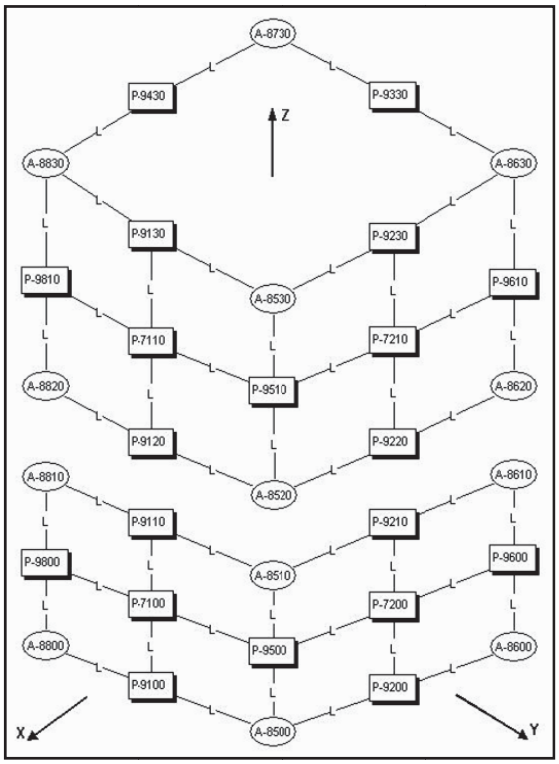

(d)

Fig. 6 Thermal network (TMM): (a) Electronic box, (b) an electronic component, (c) solar panels, (d) satellite structure

Figure 7a, b depicts the satellite in two possible orbits (here shown for $\beta=60^{o}$, 90^{o}). Table 1 presents the temperature limits of the satellite main components.

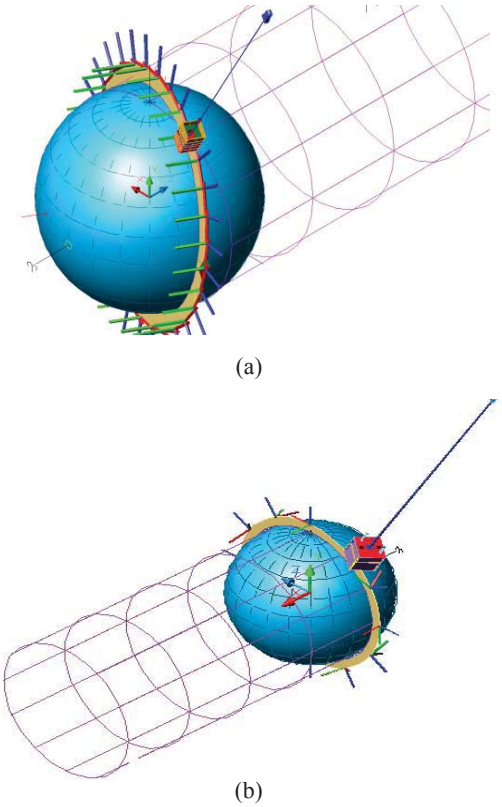

(a)

(b)

Fig.7 The satellite in its orbit: (a) β=60°, (b) β=90°

Table 1. Temperature limits of main satellite components

Unit	Operating Range (°C)	Non-operative Range (°C)
Solar Panels	-50 , +120	-
Battery Pack	-10, +25	-20, +40
Electronic Box (E-Box)	-10, +50	-40, +80
Telemetry Units	-5, +50	-50, +50
Structure	-80, +80	-

Standard software SINDA/FLUINT [21] and Thermal Desktop [22] are used in this study for the purpose of thermal modeling and analysis. The transient thermal analysis is performed through implicit forward-backward differencing given as:

$$\frac{2C_i}{\Delta t}\left(T_i^{n+1}-T_i^{n}\right) = 2Q_i + \sum_{j=1}^{N}\left[G_{ji}\left(T_j^{n}-T_i^{n}\right)+\hat{G}_{ji}\left\{\left(T_j^{n}\right)^4-\left(T_i^{n}\right)^4\right\}\right]+ \sum_{j=1}^{N}\left[G_{ji}\left(T_j^{n+1}-T_i^{n+1}\right)+\hat{G}_{ji}\left\{\left(T_j^{n+1}\right)^4-\left(T_i^{n+1}\right)^4\right\}\right] \quad (6)$$

where:

T_j^{n} = temperature of node j at the current time t

T_j^{n+1} = temperature of node i at the next time $t+\Delta t$

G_{ji} = linear conductor attaching node j to node i

$\hat{G}_{ji}$ = radiation conductor attaching node j to node i

C_i = thermal capacitance of node i

Q_i = source/sink for node i

In effect, the above finite difference equation uses the average of the temperature derivatives at the current and next time to predict the overall temperature change. and next time to predict the overall temperature change. This method is second order accurate in time and first order accurate in space [22].

Results and Discussion

Effects of Beta Angle and Altitude

In this section, effects of variation in orbit altitude, from 500 to 1000 km, and beta angles, from 0 to 90º, on satellite temperatures are presented for a nadir pointing satellite.

Figure 8 shows the variations in the temperature of the top satellite surface at various altitudes and different β angles. As shown, the top surface temperature does not vary significantly with increase or decrease in satellite altitude. This is mainly because this surface faces the zenith, which means for all β angles, it only receives solar radiation: no Earth IR or albedo radiations are received by this surface. In addition, the amount of solar radiation depends only on β angle. Therefore, increase in altitude from 700 to 1000 km has little effect on the amount of solar radiation received by this surface. The top surface, being parallel to the direction of solar rays at β= ±90º, receives no solar radiation, and hence, it reaches very low temperatures. However, at β=0º, the top surface receives the maximum amount of solar radiation during day time (the lighted part of the orbit), and attains its highest temperature at this angle. At 0º<β<±90º, the solar radiation received by the top surface gradually decreases, resulting in a downward temperature trend as illustrated in Figure 8.

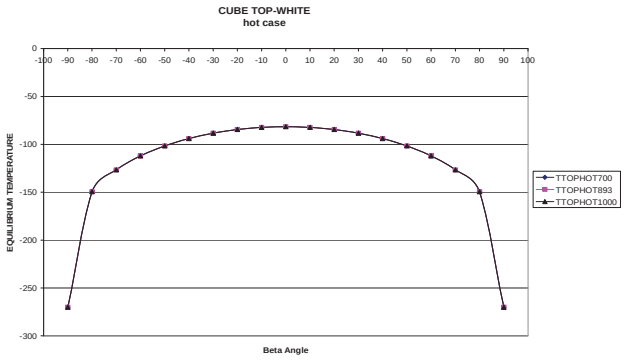

Fig. 8 Temperature variations of the top surface at various altitudes and different β angles

The temperature variations of the base plate at different altitudes and β angles are shown in Figure 9. As depicted, the temperature has decreased with increase in the altitude, reaching its minimum value at 1000 km. This observed behavior may be explained by the fact that the amounts of IR and albedo radiations received by the base plate decrease with increasing altitude, resulting in lower temperatures. In addition, for a given altitude, the Earth IR radiation shows little variation with variations in β angle and remains almost constant, while the albedo decreases with increase in β angle [1]. Since at β= ±90º, the albedo received by the base plate reaches its minimum value, this surface is mainly affected by the Earth IR radiations. Therefore, for each of the three altitudes considered in this study, the lowest temperature of the base plate occurs at β= ±90º. Also, depending on the altitude, the base plate receives the maximum amount of solar radiations at β angles ranging from ±60º to ±70º. Accordingly, maximum temperatures for the base plate occur at these β angles (see Figure 9).

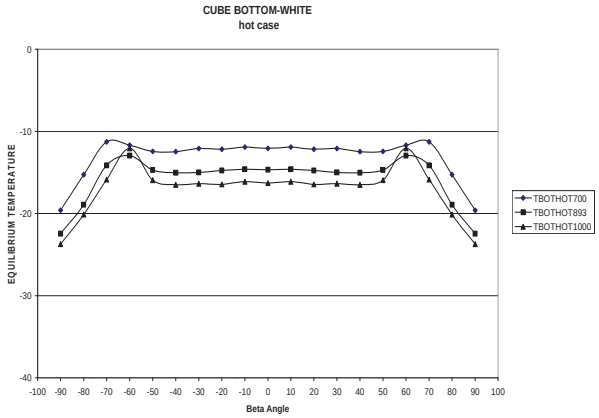

Fig. 9 Temperature variation of the base plate at different altitudes and β angles

The variations in the temperature of the satellite lateral surfaces at different altitudes and β angles are shown in Figure 10. The satellite is assumed to be a quick spun one. As shown, the four lateral surfaces, which are covered with the satellite solar panels, have attained uniform temperature profiles due to the quick spin of the satellite. The maximum and minimum amount of solar radiation received by the solar panels are obtained at β= ±90º and β= 0º, respectively. Correspondingly, as shown in this figure, the maximum and minimum temperatures of the solar panels occur at these β angles, respectively.

Figure 11 presents the battery temperatures at β=0 to 90º and 500 km orbit (for the first 20 periods). As shown, at β=70º compared to other beta angles, battery temperatures show significant difference. Figures 12 through 14 show the battery temperatures for orbit altitudes in the range of 600 to 1000 km. It may be concluded that with the increase in beta angle, battery temperatures show less variations in a particular time period, which is due to the increase in the amount of time the satellite remains exposed to the sun flux, or conversely, the decrease in the amount of time the satellite remains in the Earth shadow, with increasing the beta angle.

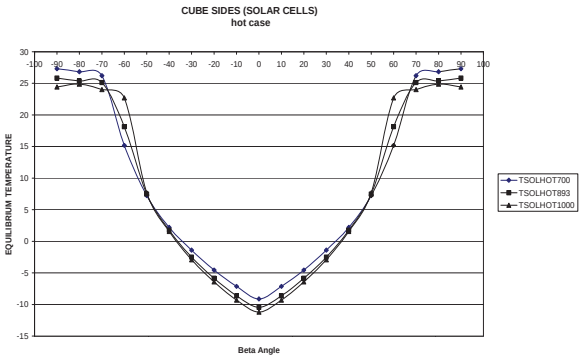

Fig. 10 Temperature variation of the lateral surfaces at different altitudes and β angles

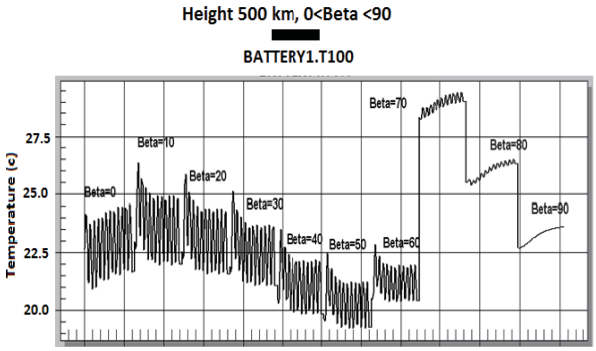

Fig. 11 Battery temperature for orbital hot case, at β=0 to 90º and 500 km altitude (for the first 20 periods)

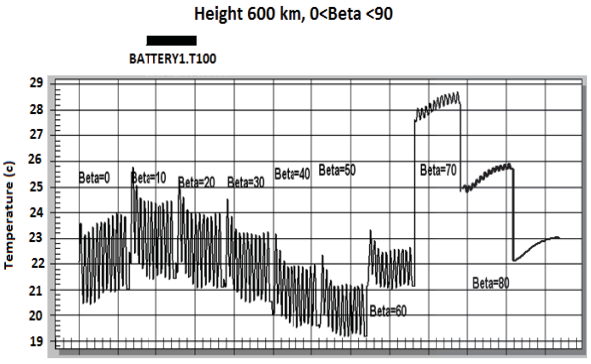

Fig.12 Battery temperature for orbital hot case, at β=0 to 90º and 600 km altitude (for the first 20 periods)

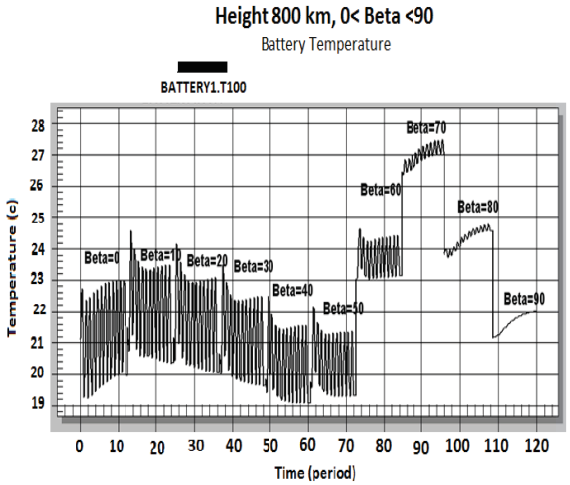

Fig. 13 Battery temperature for orbital hot case, at β=0 to 90º and 800 km altitude (for the first 20 periods)

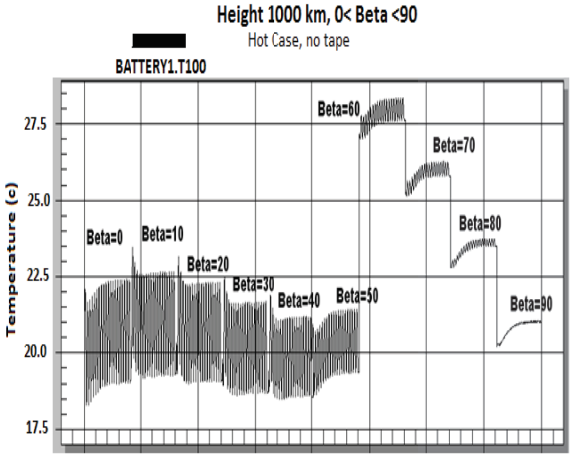

Fig. 14 Battery temperature for orbital hot case, at β=0 to 90º and 1000 km altitude (for the first 20 periods)

Comparison of the results for different altitudes shows that with the increase in altitude to 1000 km, the critical beta angel tends toward a value close to 60º. The reason for this observed phenomenon can be explained by considering environmental heat loads as shown in Figure 15 which presents the total heat flux consisting of solar, albedo and the Earth IR, absorbed by the base plate at various altitudes. As shown, the maximum heat flux pertains to β=60º at 1000 km altitude. Temperature results for an electronic unit and the base plate at β=0 to 90º and 900 km altitude are given in Figure 16. It should be mentioned that a good agreement exists between the temperatures of the electronic unit and the base plate. This surface, which acts as the satellite radiator, is influenced by the space environment and the beta angle, and depending on the amount of absorbed heat flux, it can attain various equilibrium temperatures.

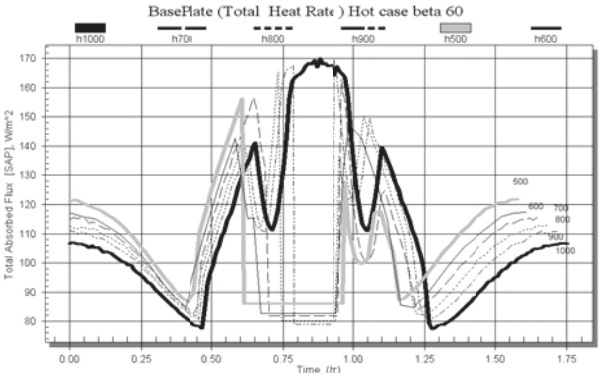

Fig. 15 Total heat flux absorbed by the base plate at various altitudes and for the hot case orbital condition

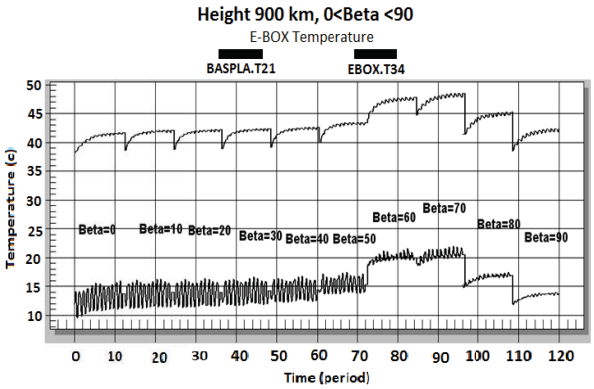

Fig. 16 Temperatures of an electronic unit and the base plate at β=0 to 90º and 900 km altitude

Temperatures of the solar panels at β=0 to 90º, with 10º increment, are shown in Figure 17. Comparison of results shows that due to the absence of eclipse and the existence of complete sunlight at β=60º and 1000 km altitude, the large temperature variations, which result from the sunlit and eclipse periods in the orbit, are reduced and the solar panel temperature variations are only due to the satellite slow spin (RPO) in the orbit.

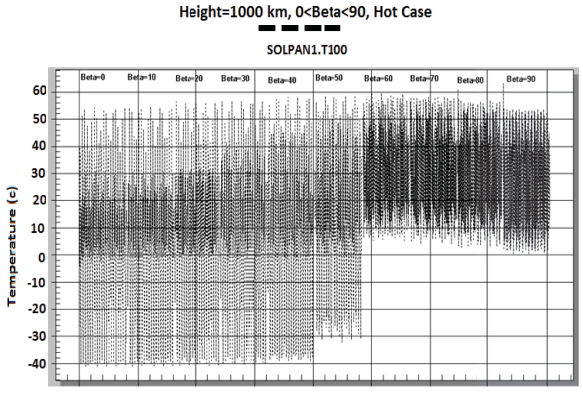

Fig. 17 Temperatures of one of the solar panels at β=0 to 90º and 1000 km altitude

Effects of Spin Rate

Figure 18 shows the limiting case of Zero Spin (RPO=0), in which a side facing the sun is heated to high temperatures (>125 ºC), and the other three sides receive no solar heat flux, and hence, are at very low temperatures (<-80 ºC). The case of zero spin presents the worst thermal condition, as all the solar panels must endure severe thermal states.

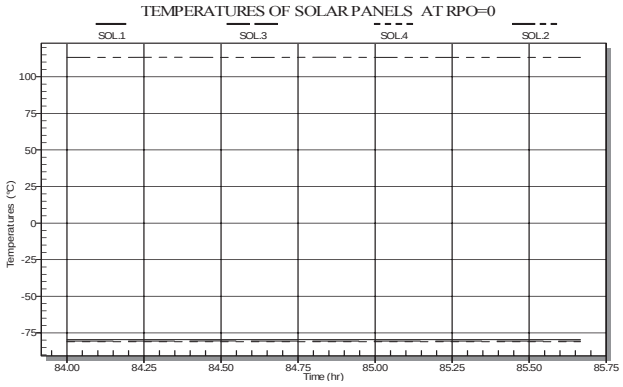

Fig. 18 Temperatures of solar panels, the no spin limiting case (RPO=0)

Solar panels temperature variations at RPO=1 and hot orbital case are shown in Figure 19. Here, the four solar panels show similar temperature variations, and the minimum temperature has increased to about -55 ºC, while the maximum temperature has decreased to about 115 ºC. However, the temperatures of the solar panels are still far from satisfactory.

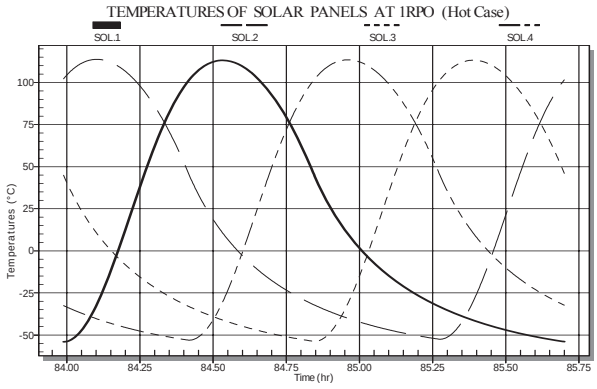

Fig. 19 Temperatures of solar panels at RPO=1

Figure 20 shows the remarkable improvement in the temperature conditions for RPO=3. The temperature range is now between -14 ºC to 78 ºC.

Solar panels temperature variations at RPO=10 and hot orbital case are demonstrated in Figure 21. It is important to note that further increase in spin rate ultimately results in the limiting case of infinite spin rate (RPO=∞). Temperatures of the four solar panels for the limiting case of quick spin (RPO=∞) are shown in Figure 22. In addition, the variations in the temperature of a single solar panel at various spin rates are depicted in Figure 23. As shown, in the case of quick spin, the maximum and minimum temperatures vanish, and the temperatures of the solar panels reach a value close to that of room temperature.

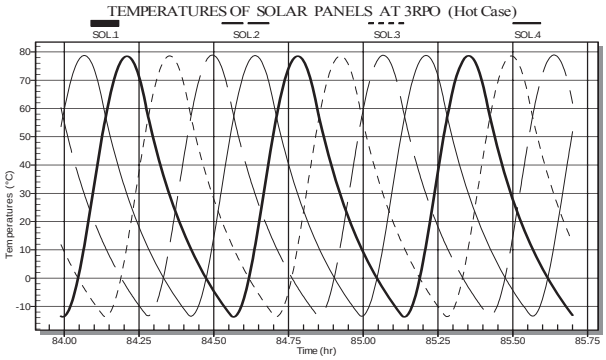

Fig. 20 Temperatures of solar panels at RPO=3

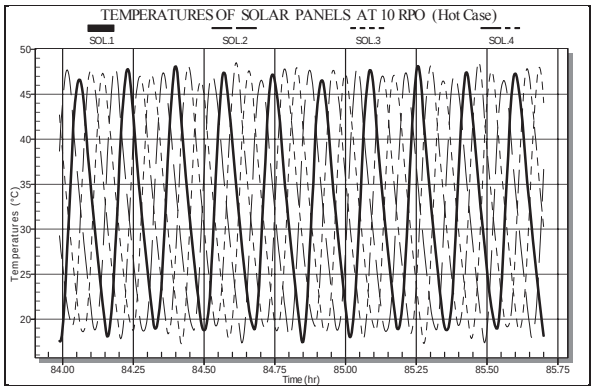

Fig. 21 Temperatures of solar panels at RPO=10

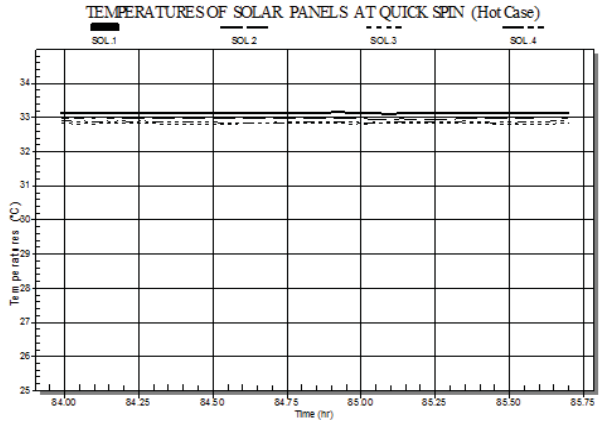

Fig. 22 Temperatures of solar panels for limiting case of quick spin (RPO=∞)

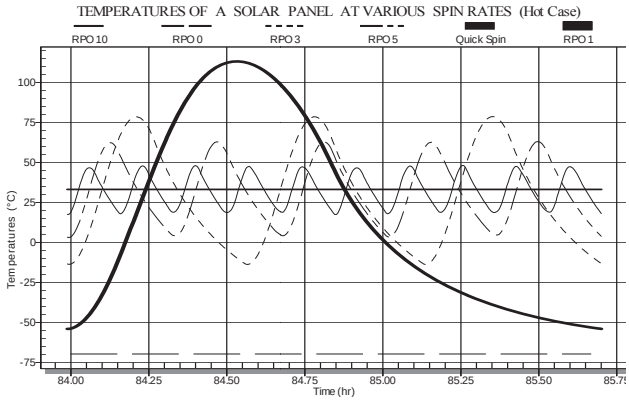

Fig. 23 Temperature variation of a single solar panel at various spin rates

The increasing spin rate diminishes both maximum and minimum temperature values. In the limit, when the spin approaches infinity, the temperatures everywhere approach the average temperature of the vehicle as required by thermodynamic equilibrium. Satellite spin can be used to improve the temperature distribution in a satellite.

A comparison of the temperature results of this study with flight temperatures results reported by Badari and Venkata Reddy [23] shows that for both cases, temperatures of the body mounted solar panels, fixed on the satellite lateral sides, match well.

Effects of Radiator Position

Temperatures of the top and bottom surfaces at β=60˚, for the two radiator positions considered in this study, are shown in Figures. 24 and 25, respectively.

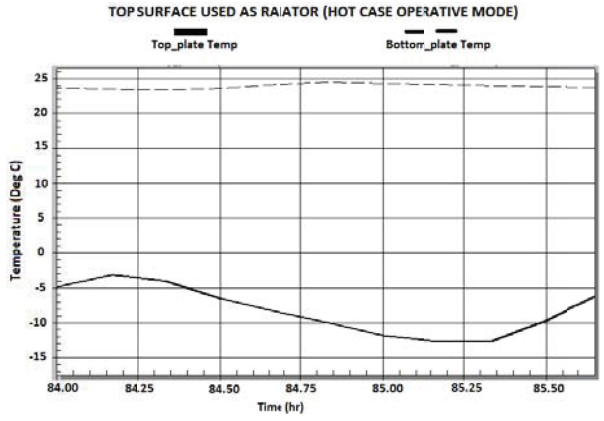

Fig. 24 Temperatures of the top and bottom surfaces at β=60º (the top radiator configuration)

(i) Top Radiator Configuration

In this configuration, the top surface, which acts as the satellite radiator, faces the deep space, and therefore, exchanges heat radiatively with the space environment. At constant internal heat dissipation, the equilibrium temperature of a radiator surface is affected by the quantity of flux, namely solar, albedo and the Earth IR, received by the surface from the environment. For the top surface (zenith facing) radiator, the albedo and IR flux will be zero, which means the radiator only receives the solar flux. This, as shown in Figure 24, results in lower temperatures of the top surface (radiator) compared to the temperature of the MLI covered bottom surface.

(ii) Bottom Radiator Configuration

For a radiator positioned at the bottom of the satellite (nadir oriented), the IR and albedo fluxes will be non-zero. In this case, the bottom surface is always nadir pointing and the radiator will receive albedo and the Earth IR heat flux. Hence, in general, the radiator temperature will be higher for the bottom surface radiator configuration (see Figure 25). This means that the temperatures of various components in the satellite, depending on their relative positions with respect to the satellite radiator, will be higher for the bottom surface radiator configuration than the top surface radiator configuration.

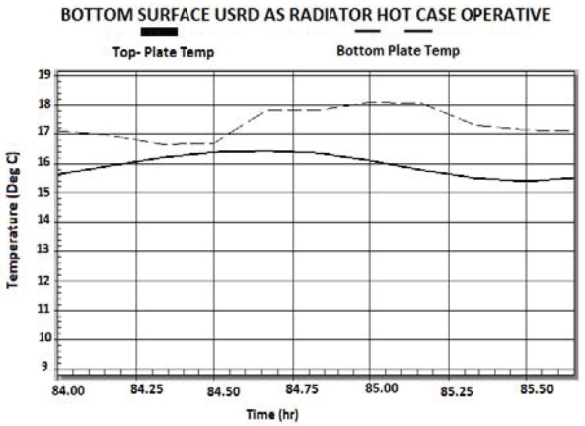

Fig. 25 Temperatures of the top and bottom surfaces at β=60º (the bottom radiator configuration)

Conclusion

The following conclusions can be drawn from the results:

- Change in the satellite altitude, in the range considered in this study, does not produce critical thermal conditions, and hence, passive thermal control can still be used with sufficient reliability.
- Spin rate has a marked influence on the satellite temperature distribution. Spin rate equal to or greater than 3 RPO will result in good overall temperature distribution in the satellite solar panels.
- The maximum and minimum temperatures vanish in the quick spin case; the temperatures of the solar panels approach room temperature.

- The top surface radiator configuration results in lower temperatures as compared to the bottom surface configuration, and therefore, it could be the preferred configuration for small satellites with similar shapes and mission requirements.
- Comparison of the results with flight temperatures results reported by other researches indicates the adequacy of the discussed considerations for use in the design of satellites of similar configurations, missions and orbital parameters.

References

[1] Gilmore, D.G., *Spacecraft Thermal Control Handbook*, Vol. I*: Fundamental Techniques*, The Aerospace Corporation Press, 2002.

[2] Griffin, M.D. and French., J.R., *Space Vehicle Design*, Copyright© AIAA, Washington, DC, 1991.

[3] Martin, D., *Parametric Models and Optimization for Rapid Thermal Design*, MicroSat Systems Inc., Copyright© SAE International, 2004.

[4] *Earth's Thermal Environment, Thermal Environments*, JPL D-8160, K&K Associates, 2008.

[5] *Orbit Definition*, Structural Dynamics Research Corporation, 2001.

[6] Abouel-Fotouh, A.M, Elsharkawy, A.I., Shabaka, I. and Elfar, A., "The Effect of Satellite Orientation on Satellite Surface Temperature Distributions", *Journal of Applied Sciences Research*, Vol. 2, No.12, 2006, pp.1286-1292.

[7] *Method for the Calculation of Spacecraft Umbra and Penumbra Shadow Terminator Points*, NASA Technical Paper 3547, 2002.

[8] Wertz, J.R. and Wiley J.L., *Space Mission Analysis and Design*, Microcosm Press, El Segundo CA, 1999, pp. 428-458.

[9] Eakman, D., Lambeck, R. and Slofer, L., Jr., *Small Spacecraft Power and Thermal Subsystems*, NASA Contractor Report 195029, Contract NASI-19244, Task 15, 1994.

[10]Silverman, E. M., *Space Environmental Effects on Spacecraft: LEO Materials Selection Guide*, NASA Contractor Report 4661, Parts 1 and 2, Prepared for Langley Research Center, 1995.

[11]Petrof, R.C. and Raynor S., "The Temperature Distribution in Rotating Thick-Walled Cylinders Heated by Radiation", *International Journal of Heat & Mass Trans.*, Vol. 11, Issue 3, 1968, pp. 427-438.

[12]Gadalla, M.A., "Analytical Modeling of Thermal Analysis of Rotating Space Vehicles Subjected to Solar Radiation", *Trans. Energy Conversion, American Chemical*, 1993.

[13]Olmstead, W.E. and Raynor S., "Solar Heating of a Rotating Solid Cylinder", *Quarterly of Applied Mathematics*, 1963, pp. 81-90.

[14]Nichols, L.D., *Surface Temperature Distribution on Thin-walled Bodies Subjected to Solar Radiation in Interplanetary Space*, NASA Technical Note D-584, USA, 1961.

[15]Gadalla, M. "Prediction of Temperature Variation in a Rotating Spacecraft in Space Environment," *Applied Thermal Engineering*, Vol. 25, No. 14-15, 2005, pp. 2379-2397.

[16]Anvari, A., Farhani, F., Entezari, M.H. and Niaki, K.S., "Modeling and Thermal Analysis of Satellite Solar Panels", *The 8th Iranian Aerospace Society Conference (IAS2009)*, Malek-E-Ashtar University, Esfahan, Iran, 2009, (In Persian).

[17]*Design of Hardware and Software for the Power Supply for AAU CubeSat*, Appendix B, Group 02gr 733, 2002.

[18]Karam, R.D., *Satellite Thermal Control for Systems Engineers*, Vol. 181, Progress in Astronautics and Aeronautics, AIAA, Virginia, USA, 1998.

[19]Baturkin, V., "Micro-Satellite Thermal Control Concepts and Components", *ACTA Astronautica*, Vol. 56, No.1-2, 2003, pp. 161-170.

[20] Galski, R.L., de Sousa, F.L., Ramos, F.M. and Muraoka, I., "Spacecraft Thermal Design with the Generalized External Optimization Algorithm," Inverse Problems, *Design and Optimization Symposium*, Rio de Janeiro, Brazil, 2004.

[21]*SINDA/FLUINT User's Manual*, Version 4.4, Cullimore and Ring Technologies Inc., 2001.

[22]Panczak T.D., *Thermal Desktop*, Version 4.4, Cullimore and Ring Technologies Inc., 2001.

[23]Badari and Venkata Reddy, "Thermal Design and Performance of HAMSAT," *Acta Astronautica*, Vol. 60, Issue 1, 2007, pp. 7-16.